Individual Phase Current Control Based on Optimal Zero-Sequence Current Separation for a Star-Connected Cascade STATCOM Under Unbalanced Conditions

Youjie Shi, Bangyin Liu, *Member, IEEE*, Yanjun Shi, *Member, IEEE*, and Shanxu Duan

***Abstract*—This paper proposes an individual phase current control (IPCC) method based on optimal zero-sequence current separation for star-connected cascade STATCOMs under unbalanced grid voltage. The IPCC is adopted to get better adaptation to unbalanced conditions. Each cluster of the cascade STATCOM has its own phase current control loop and dc-voltage feedback loop, and it can generate the necessary negative-sequence current automatically to rebalance power. However, the zero-sequence current which is unnecessary and harmful in star configuration is introduced in the process. An optimal zero-sequence current separation is presented to remove the zero-sequence current by reconstructing the reactive current command. This improved IPCC enables star-connected STATCOMs adapt to unbalanced conditions without the need for any power balancing algorithms. Also, the operation range of the proposed control method is analyzed. Simulation research studies are performed to verify the operation range analysis, and the experimental operation is tested on a 25-level ±10 Mvar/10-kV STATCOM product installed at a wind farm.**

***Index Terms*—Cascade multilevel converter (CMC), individual phase current control (IPCC), star configuration, static synchronous compensator (STATCOM), unbalanced operation.**

I. Introduction

CASCADE multilevel converter (CMC) topology is very attractive in high-power-level applications because of its increased voltage rating, high equivalent switching frequency, and improved harmonic performance [1]–[8], especially in STATCOMs (STATic synchronous COMpensators) where dc sources are no longer needed [9]–[16]. The circuit structure of a star-connected cascade STATCOM is shown in Fig. 1. All STATCOMs have to deal with the unbalanced grid condition [17], [18] which is usually caused by the unbalanced load, asymmetry fault, or resonating reactive power on the transmission line. STATCOMs are supposed to provide reactive power rather than shut down or just "ride through" like other grid-connected devices. Besides dc-link ripple and ac-side overcurrent, a cascade STATCOM may also suffer dc-voltage unbalance due to its separated dc links [19], [20]. Moreover, the star configuration needs more complicated control for unbalanced conditions, because it has a floating neutral point.

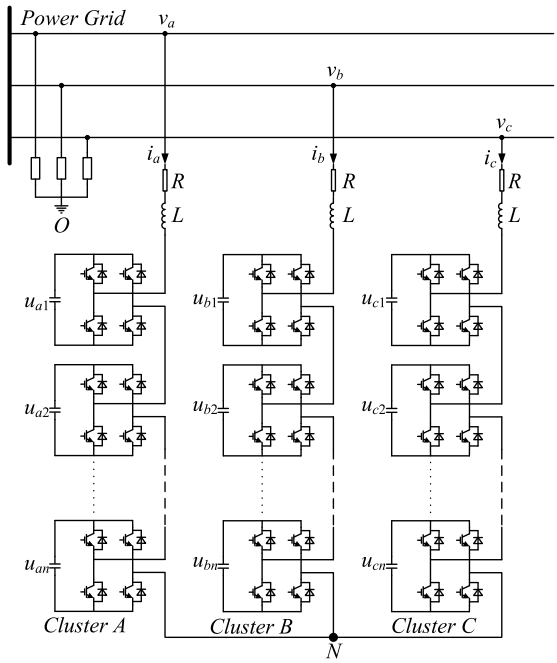

Fig. 1. Circuit configuration of a star-connected cascade STATCOM.

Basically, there are two kinds of control methods for unbalanced operating cascade STATCOMs with star configuration, namely the zero-sequence voltage injection (ZSVI) [20]–[26], and the negative-sequence current injection (NSCI) [27]–[30]. ZSVI, also called neutral shift, controls the active power distribution among three phases by shifting the floating neutral point voltage, therefore, maintaining the balanced dc voltages among each phase converter (also called a cluster). Maharjan *et al.* [22] use ZSVI in a CMC-based battery energy storage system. The zero-sequence voltage is calculated based on power balancing instead of voltage feedback. Therefore, this method is more suitable for applications with batteries on dc links than STATCOMs. In [20], each cluster has a dc-voltage feedback, and clear explanation and demonstration of how to calculate the zero-sequence

Manuscript received December 15, 2014; revised March 30, 2015; accepted May 21, 2015. Date of publication June 8, 2015; date of current version November 16, 2015. This work was supported by the National Natural Science Foundation of China under Project 51361130150. Recommended for publication by Associate Editor J. H. R. Enslin

Y. Shi, B. Liu, and S. Duan are with the State Key Laboratory of Advanced Electromagnetic Engineering and Technology, School of Electrical and Electronic Engineering, Huazhong University of Science and Technology, Wuhan 430074, China (e-mail: shiyjhust@hust.edu.cn; lby@hust.edu.cn; duanshanxu@hust.edu.cn).

Y. Shi is with the Center for Advanced Power Systems, Florida State University, Tallahassee, FL 32310 USA (e-mail: yshi3@fsu.edu).

Color versions of one or more of the figures in this paper are available online at http://ieeexplore.ieee.org.

Digital Object Identifier 10.1109/TPEL.2015.2442528

compensating voltage as well as an operation range analysis of ZSVI are provided. However, in [20], ZSVI is performed by one cluster, and the analysis is only based on the balanced grid voltage. The authors in [23]–[26] realize cluster-balancing control by injecting a common zero-sequence voltage into the clusters of STATCOM. The problem of ZSVI is that it causes extra voltage stress on some cluster, and needs a wide margin for dc-capacitor voltage, leading to a tradeoff between the cost and available operation area [25]. On the other hand, as a counterpart and alternative, NSCI was first used in an active power filter for load balancing [27]. A negative-sequence current control loop is usually used to generate proper negative-sequence output current and rebalance three-phase powers [28], [29]. It puts little extra voltage stress on clusters, but sets a strict constrain on the ratio of three-phase currents, and disturbs the control of the output current waveform. Therefore, some researchers combine two methods together [30], [31], and switch them ON and OFF according to operation conditions, which further complicates the problem.

Generally, dq-axis or $\alpha\beta$-axis control is adopted in most feedback techniques for cascade STATCOMs. Under unbalanced conditions, low-frequency harmonic components are involved in the controller. Positive- and negative-sequence extraction or low-pass filters are employed by some methods, but time delay and limited stability range are also introduced. There is another way to solve the problem. By simply being treated as three individual single-phase converters, three clusters control their own dc voltage and track own current reference, and the cascade STATCOM can spontaneously generate positive-, negative-, and zero-sequence current, exchanging the unbalanced power. This method is called individual phase current control (IPCC). ALSTOM designed a cascade STATCOM under IPCC [32], [33] which had strong adaptability to unbalanced system, but with slow reactive power response speed. The authors in [34] and [35] improve IPCC based on instantaneous current control, which can dramatically shorten the transient duration and enhance the waveform control capability. Nevertheless none of them focuses on the unbalanced operation of star configuration. The authors in [36] apply IPCC to a star-connected cascade STATCOM industrial prototype but without considering the unbalanced operation. The authors in [37] propose a sliding-mode variable structure controller which combines direct feedback linearization control and IPCC together; however, the control strategy is complex, and the zero-sequence issue is not solved.

Though the star-connected cascade STATCOM under IPCC is naturally equipped with adaptation to unbalanced grid, the problem is that since three-phase controllers are independent to each other, they generate not only positive and negative but also zero-sequence current which is not allowed in three-wire systems. In this paper, an algorithm called optimal zero-sequence current separation (OZSCS) is proposed to remove the zero-sequence current and improve the IPCC. By applying IPCC along with OZSCS, the star-connected cascade STATCOM can be adapted to unbalanced grid conditions automatically without demands for any extra power balancing algorithms. The rest of this paper is organized as follows: in Section II, a control structure illustrating the proposed IPCC for unbalanced conditions is given, along with the presentations of the OZSCS and individual phase lock loop (PLL). In Section III, the operation range of the proposed control method is analyzed by finding out the voltage stress and the negative-sequence current proportion under certain unbalanced condition, as well as the constraints of OZSCS algorithm itself. Section IV gives simulation verifications performed on PSCAD and experimental verifications on a $\pm$10 Mvar/10-kV STATCOM product. Finally, conclusions are drawn in Section IV.

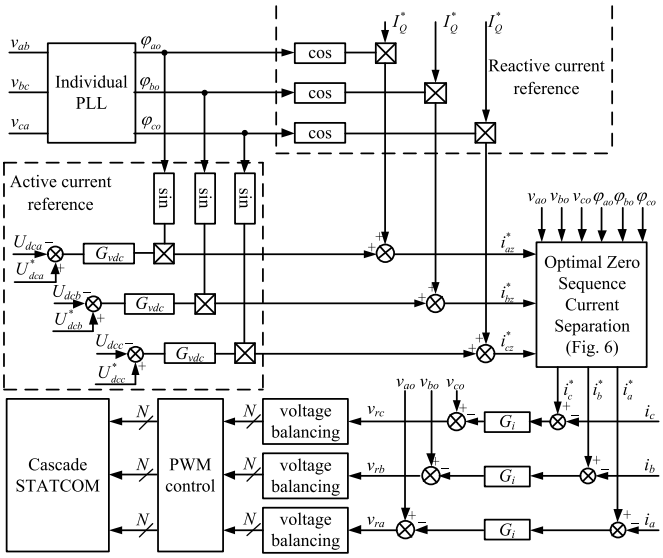

Fig. 2. Individual phase instantaneous current control scheme.

II. Control Strategy

A. General Description

The control method of star-connected cascade STATCOMs is shown in Fig. 2. The reactive current reference comes from an upper layer control, usually a reactive power scheduling table or a grid voltage controller. G_{vdc} controls the average dc voltage of each cluster individually, generating the active part of the current reference. The instantaneous total current reference is obtained by adding reactive and active components together. When the grid voltage is unbalanced, G_{vdc} of each cluster will generate different active reference in order to maintain own average dc-voltage constant. Therefore, the positive, negative, and zero sequence can all exist in the instantaneous current reference. Thus, the following module, OZSCS, is introduced to get rid of the unnecessary zero-sequence current reference component. G_i controls the instantaneous grid current of each cluster individually to track own current reference. The cell dc-voltage balancing control proposed in [35] and [38] is used to balance the dc voltages of different cells in one cluster, which is not the focus of this paper. The individual PLL detects the voltage phase angle of each cluster. Note that the voltage reference O used here to convert line-to-line voltages into phase voltages is specially chosen to guarantee that there is no zero-sequence component in the phase voltage.

OZSCS is a crucial part of the proposed method because: 1) it has to make sure that there is no zero-sequence component in the current reference in star configuration; 2) this separation module should not influence either current control or dc-voltage control. These two constrains are theoretically compatible because the negative-sequence current alone is enough to rebalance the power among three clusters and the zero-sequence current reference is just a "side effect" produced by individual phase instantaneous current control.

Another important issue is PLL. In STATCOM application where dynamic response is required, software PLL based on synchronous reference frame (SRF) is more preferable to the traditional zero cross detection PLL. But large unbalanced condition will cause failure to the conventional SRF-based PLL. And the IPCC method requires the phase angle of each phase grid voltage, even under unbalanced conditions. This particular requirement has ruled out a lot of modified SRF PLLs capable of tracking unbalanced voltage, because they only give the phase angle of positive-sequence voltage. Therefore, in this paper, a modified SRF PLL based on virtual three phase is applied.

B. OZSCS

The object of the OZSCS algorithm is to remove the zero-sequence component in the current reference without influencing other control loops. There are several issues that should be considered when designing this OZSCS algorithm.

1) Change Only the Reactive Part of the Reference: For a given set of current reference $[i_{az}^*, i_{bz}^*, i_{cz}^*]^T$ containing zero sequence, one can always get a set of reference without zero-sequence component, namely $[i_a{}^*, i_b{}^*, i_c{}^*]^T$, by slightly changing the value of $[i_{az}{}^*, i_{bz}{}^*, i_{cz}{}^*]^T$. It is important to make sure that this change only affects the reactive output. Because in STATCOM where there are no dc sources, slight changes in the active power will greatly influence the dc voltages. It means in Fig. 3(a), the current phasors $\mathbf{I}_{\mathrm{az}}{}^*$, $\mathbf{I}_{\mathrm{bz}}{}^*$, $\mathbf{I}_{\mathrm{cz}}{}^*$ can only be moved along the dashed lines.

2) Changes in reference should be minimized: The idea shown in Fig. 3(a) can be further expressed as Fig. 3(b), where $\mathbf{I}_{\mathrm{z}}{}^*$ stands for the zero-sequence component in the current reference, given by

$$\mathbf{I}_z^* = \mathbf{I}_{az}^* + \mathbf{I}_{bz}^* + \mathbf{I}_{cz}^* \tag{1}$$

The task is to use a set of segments with certain length on the dashed lines, namely $\mathbf{I}_{\mathrm{a}}{}^* - \mathbf{I}_{\mathrm{az}}{}^*$, $\mathbf{I}_{\mathrm{b}}{}^* - \mathbf{I}_{\mathrm{bz}}{}^*$, and $\mathbf{I}_{\mathrm{c}}{}^* - \mathbf{I}_{\mathrm{cz}}{}^*$, to create a $-\mathbf{I}_{\mathrm{z}}{}^*$ to cancel $\mathbf{I}_{\mathrm{z}}{}^*$. Since the whole idea of this method is making some variation in the reactive current command, it is important to keep this variation minimized, i.e., in Fig. 3(b), to make the sum of three modification phasors $|\mathbf{I}_{\mathrm{a}}{}^* - \mathbf{I}_{\mathrm{az}}{}^*| + |\mathbf{I}_{\mathrm{b}}{}^* - \mathbf{I}_{\mathrm{bz}}{}^*| + |\mathbf{I}_{\mathrm{c}}{}^* - \mathbf{I}_{\mathrm{cz}}{}^*|$ shortest.

The sector location algorithm is given in Fig. 4. By moving three dashed lines in Fig. 4 to the point O, the plane can be divided into six sectors. The task in Fig. 3(b) is now updated to find the shortest segments on the dashed lines to form the vector $-\mathbf{I}_{\mathrm{z}}{}^*$ in Fig. 4. The solution is to use only the edges of sector in which $-\mathbf{I}_{\mathrm{z}}{}^*$ is located. For example, if $-\mathbf{I}_{\mathrm{z}}{}^*$ is in Sector III, only use the segments on $\mathbf{oa}$ and $\mathbf{ob}'$ to form the vector $-\mathbf{I}_{\mathrm{z}}{}^*$. This will guarantee that $-\mathbf{I}_{\mathrm{z}}{}^*$ is formed by the smallest variation of reactive current reference.

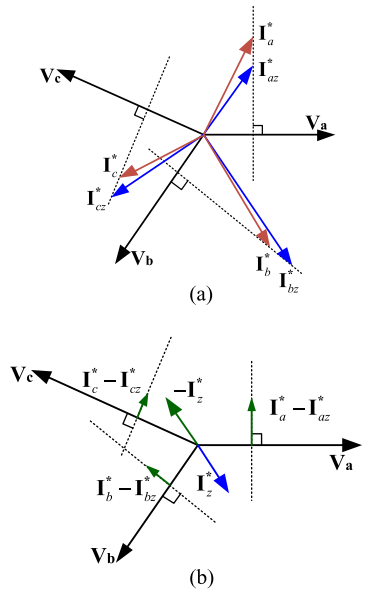

Fig. 3. Phasor diagram showing the idea of zero-sequence separation changing only the reactive current. (a) $[\mathbf{I}_{\mathrm{az}}{}^*, \mathbf{I}_{\mathrm{bz}}{}^*, \mathbf{I}_{\mathrm{cz}}{}^*]$: three-phase current with zero sequence; $[\mathbf{I}_{\mathrm{a}}{}^*, \mathbf{I}_{\mathrm{b}}{}^*, \mathbf{I}_{\mathrm{c}}{}^*]$: three-phase current without zero sequence. (b) Using phasors on the dashed lines to form $-\mathbf{I}_{\mathrm{z}}{}^*$.

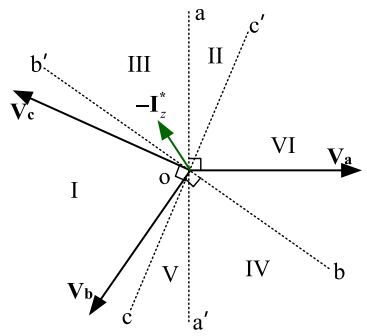

Fig. 4. Sector location algorithm and definition of sectors.

The method of locating $-\mathbf{I}_{\mathrm{z}}{}^*$ is to judge which side $-\mathbf{I}_{\mathrm{z}}{}^*$ is on referring to each dashed line. For example, if $-\mathbf{I}_{\mathrm{z}}{}^*$ is on the left side of aa', on the left side of bb', and on the right side of cc', then $-\mathbf{I}_{\mathrm{z}}{}^*$ must be in Sector III. This can be realized easily in a digital controller. In digital realization, only the signs of the instantaneous value of $-\mathbf{I}_{\mathrm{z}}{}^*$ and three-phase grid voltages (referring to previously defined point O) are needed. It can be coded as a three-bit value referring to the sector number, as shown in Table I.

After the sector location, the remaining work is just to solve a geometrical problem shown in Fig. 5, i.e., to find out $|\mathbf{ox}|$, $|\mathbf{oy}|$ by using $|-\mathbf{I}_{\mathrm{z}}{}^*|$, φ_x, φ_y, and φ_z.

Solve the following equation

$$\begin{cases} |\mathbf{ox}| \cdot \sin(\varphi_x) + |\mathbf{oy}| \cdot \sin(\varphi_y) = |-\mathbf{I}_{\mathbf{z}}^*| \cdot \sin(\varphi_z) \\ |\mathbf{ox}| \cdot \cos(\varphi_x) + |\mathbf{oy}| \cdot \cos(\varphi_y) = |-\mathbf{I}_{\mathbf{z}}^*| \cdot \cos(\varphi_z) \end{cases} \tag{2}$$

TABLE I
SECTOR LOCATION ALGORITHM

Sector	sign($-\mathrm{I_z}^*$) XOR sign($\mathrm{V_c}$)	sign($-\mathrm{I_z}^*$) XOR sign($\mathrm{V_b}$)	sign($-\mathrm{I_z}^*$) XOR sign($\mathrm{V_a}$)	Sector NO.
b'oc	0	0	1	I
aoc'	0	1	0	II
aob'	0	1	1	III
a'ob	1	0	0	IV
a'oc	1	0	1	V
boc'	1	1	0	VI

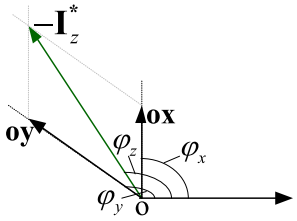

Fig. 5. Equivalent solution of OZSCS.

and get

$$\begin{pmatrix} |\mathbf{ox}| \\ |\mathbf{oy}| \end{pmatrix} = \begin{pmatrix} -\dfrac{|-\mathbf{I}_\mathbf{z}^*|\cos(\varphi_y)\sin(\varphi_z) - |-\mathbf{I}_\mathbf{z}^*|\sin(\varphi_y)\cos(\varphi_z)}{\cos(\varphi_x)\sin(\varphi_y) - \sin(\varphi_x)\cos(\varphi_y)} \\ \dfrac{|-\mathbf{I}_\mathbf{z}^*|\cos(\varphi_x)\sin(\varphi_z) - |-\mathbf{I}_\mathbf{z}^*|\sin(\varphi_x)\cos(\varphi_z)}{\cos(\varphi_x)\sin(\varphi_y) - \sin(\varphi_x)\cos(\varphi_y)} \end{pmatrix} \quad (3)$$

Therefore, the smallest set of vectors which is used for zero-sequence separation is shown in equation (4). Note that in this paper, the expression of the grid voltage is assumed as a sine function

$$\begin{pmatrix} \mathbf{ox} \\ \mathbf{oy} \end{pmatrix} = \left[\begin{pmatrix} |\mathbf{ox}| \\ |\mathbf{oy}| \end{pmatrix} \circ \begin{pmatrix} \cos(\varphi_x - \frac{\pi}{2}) \\ \cos(\varphi_y + \frac{\pi}{2}) \end{pmatrix} \right]$$

$$= \begin{pmatrix} |-\mathbf{I}_\mathbf{z}^*| \cdot \dfrac{\sin(\varphi_x)\cos(\varphi_y)\sin(\varphi_z) - \sin(\varphi_x)\sin(\varphi_y)\cos(\varphi_z)}{\sin(\varphi_x - \varphi_y)} \\ |-\mathbf{I}_\mathbf{z}^*| \cdot \dfrac{\cos(\varphi_x)\sin(\varphi_y)\sin(\varphi_z) - \sin(\varphi_x)\sin(\varphi_y)\cos(\varphi_z)}{\sin(\varphi_x - \varphi_y)} \end{pmatrix} \quad (4)$$

In equation (4), $x, y \in \{a, a^{'}, b, b^{'}, c, c^{'}\}$, depending on which sector $-\mathbf{I}_z{}^*$ is currently in $\varphi_x, \varphi_y \in \{\varphi_{ao} + \pi/2, \varphi_{bo} + \pi/2, \varphi_{co} + \pi/2\}$. Add the instantaneous values given by equation (4) to the current reference $[i_{az}{}^*, i_{bz}{}^*, i_{cz}{}^*]^T$, and then, a new set of zero-sequence-free reference $[i_a{}^*, i_b{}^*, i_c{}^*]^T$ with minimized change in and only in the reactive part is obtained. φ_{ao}, φ_{bo}, φ_{co}, and φ_z are all obtained by using virtual three-phase-based individual PLL technique. The control scheme of this optimal zero-sequence current reference separation is shown in Fig. 6.

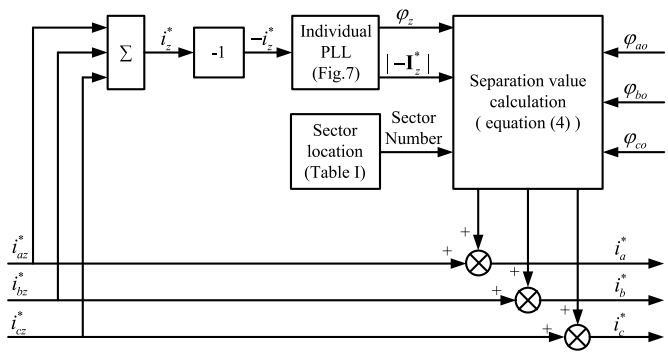

Fig. 6. Control scheme of optimal zero-sequence current reference separation.

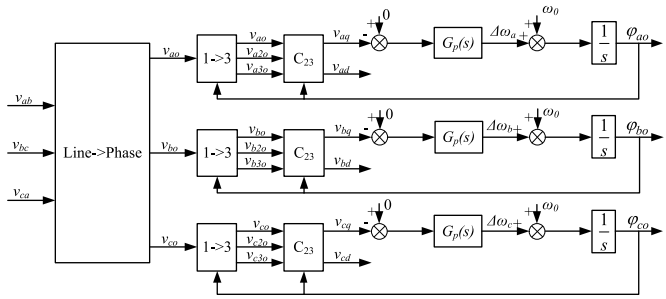

Fig. 7. Control scheme of individual PLL based on virtual three-phase dq transformation.

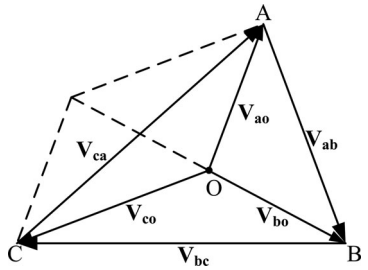

Fig. 8. Phasor diagram defining voltage reference point O.

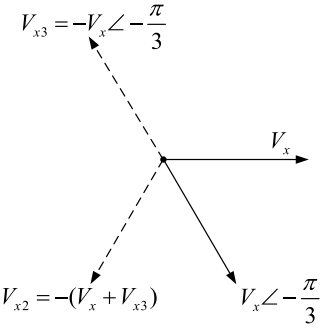

Fig. 9. Using one-phase instantaneous voltage to generate virtual three-phase voltages.

C. Individual PLL

The individual PLL used in this paper is shown in Fig. 7. By applying virtual three-phase technique shown in Fig. 9, each phase is locked individually. Different from other SRF-based PLLs, this PLL method gives out the phase angle of each phase voltage, instead of the phase A angle of the positive-sequence

voltage. This can make the unbalanced voltage have no influence on converter control.

The line-to-phase conversion module is used to convert the line-to-line voltages into phase voltages referring to the only reference point O which can make the three-phase voltages contain no zero-sequence component. This point O exists and is unique which therefore makes it a convenient reference point. The existence and uniqueness can be explained in Fig. 8. In ΔABC formed by three line-to-line voltages, the Centroid O is the only point that can make **AO**, **BO**, **CO** (standing for any set of three-phase voltages) form a triangle again (meaning no zero sequence) just by parallel translation. Therefore, the calculation of $\mathbf{V_{ao}}, \mathbf{V_{bo}}$, and $\mathbf{V_{co}}$ can be given in equation (5) by the property of triangle centroid

$$\begin{bmatrix} \mathbf{V_{ao}} \\ \mathbf{V_{bo}} \\ \mathbf{V_{co}} \end{bmatrix} = \frac{1}{3} \begin{bmatrix} V_{ab} - V_{ca} \\ V_{bc} - V_{ab} \\ V_{ca} - V_{bc} \end{bmatrix} \tag{5}$$

Fig. 9 shows the method of using the single-phase voltage to generate virtual three-phase voltages. By using the instantaneous value of one-phase voltage and the value from one-sixth line period ago, a set of balanced three-phase voltages can be constructed. Then, as shown in Fig. 7, perform dq transformation to each set of virtual three-phase voltages and make the q-axis value to be zero by feedback control. ω_o is the line frequency that defines the central frequency around which the PLL locks to. By using $-\mathbf{I}_z^*$ as the input, φ_z can also be obtained in the same way.

III. Operation Range Analysis

This section aims to find out what level of unbalance can a STATCOM withstand under IPCC based on OZSCS. The injected negative-sequence current may occupy a part of current rating, so the unbalance level of the output current should be analyzed for evaluating the reactive compensation capacity of the STATCOM under IPCC. Besides, for a STATCOM which is controlled as a current source, like in this study, overvoltage is the reason that causes it to disconnect from the grid, because the overcurrent can be avoided by limiting the current or blocking driving signals temporarily. Therefore, the unbalance operation range is not only affected by the OZSCS algorithm itself, but also limited by the voltage stress.

A. Proportion of the Injected Negative-Sequence Current

For a star-connected cascade STATCOM, the potential of the neutral point N in Fig. 1 is essential to determine the voltage stress. The IPCC does not need to change the neutral potential for power balancing, so the point N stays at its "original" place in the line-to-line voltage triangle. In the IPCC method, each cluster has the same controller; therefore, the close loop impedances of three clusters are same. It can be easily proved (by using the superposition principle of circuit theory) that for a star-connected network with balanced impedances, the line-to-neutral voltages (also called phase voltages) can meet equation

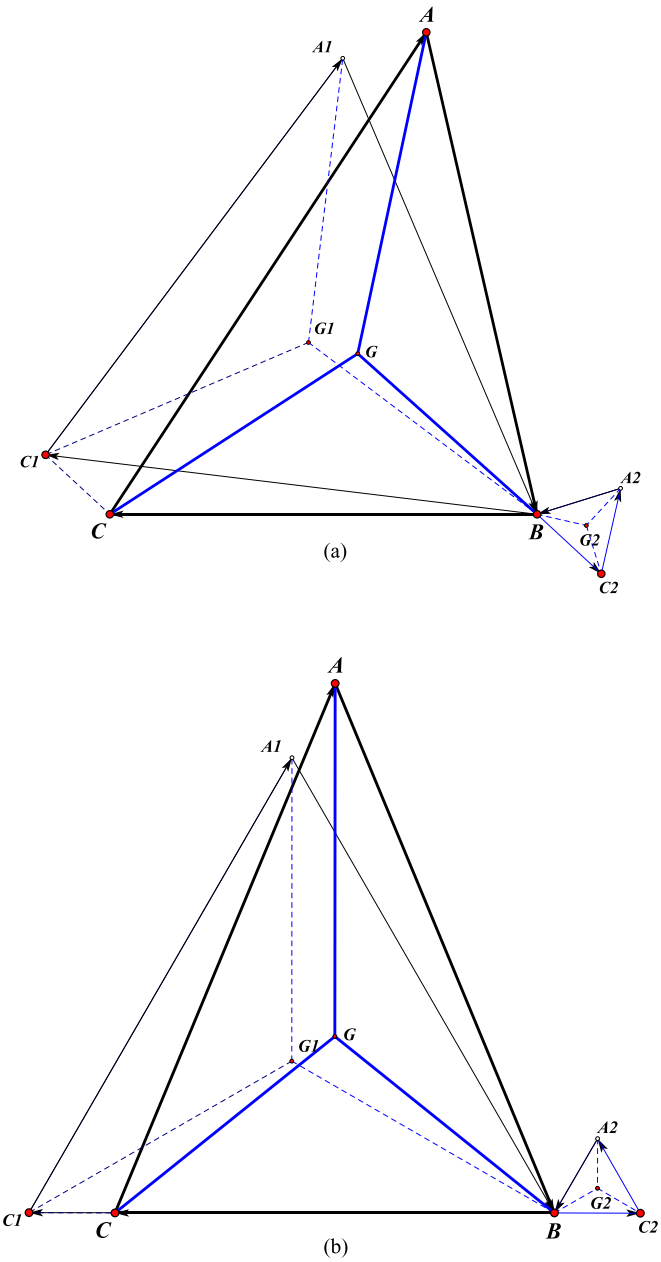

Fig. 10. Line-to-line voltage triangle, positive-sequence triangle, and negative-sequence triangle. (a) General condition. (b) Maximum voltage stress condition.

(5). It means that the "original" place of point N is at the **Centroid** of ΔABC, the same place with the grid voltage reference point O (see ΔABC in Fig. 8). Note that the potential of the neutral point N and phase voltage reference point O do not always need to be at the same point. For example, in ZSVI methods for power balancing, the neutral point N is at the Fermat point of ΔABC and the phase voltage reference O can still be at the centroid.

In Fig. 10(a), the line-to-line voltage triangle ΔABC can be decomposed into the positive- and negative-sequence triangle, namely $\Delta \mathrm{A_1BC_1}$ and $\Delta \mathrm{A_2BC_2}$. G, $\mathrm{G_1}$, and $\mathrm{G_2}$ are the centroids of three triangles, respectively. Due to the none-zero-sequence-current constrain in star-connected STATCOMs, three-phase

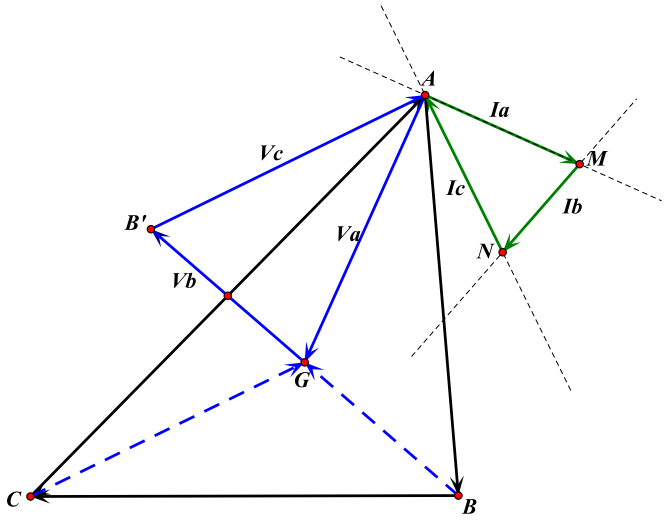

Fig. 11. Line-to-line voltage triangle, phase voltage triangle, and grid current triangle.

grid current phasors can form a triangle as well. As shown in Fig. 11, ΔAGB' and ΔAMN stand for the phase voltage triangle and grid current triangle, respectively. In the steady state, the active current components can be ignored because of the negligible power losses, hence, three grid currents are approximately vertical with each phase voltage. It is easy to find out that ΔAGB' and ΔAMN are similar triangles for having equal interior angles.

Define the unbalance factor of the line voltage as $k = V_-/V_+$ [39], where V_+ and V_- are the amplitudes of the positive- and negative-sequence components of the line voltage, namely the lengths of A_1C_1 and A_2C_2 in Fig. 10. It can be proved mathematically that the line-to-neutral voltage shares the same unbalance factor with the line-to-line voltage, namely the value of V_n/V_p equals k as well, where V_p and V_n are the amplitudes of the positive- and negative-sequence components of the phase voltage, or the length of A_1G_1 and A_2G_2 in Fig. 10. Besides, the value of the grid current unbalance factor is same with the one of phase voltage because they have similar phasor triangles. Hence, in the grid current, the ratio of the negative- and positive-sequence components equals k:1. The proportion of the injected negative-sequence current is totally determined by the grid unbalance level.

B. Voltage Stress Analysis

The problem can be described as: for a certain unbalance factor k, how much is the voltage stress? Define the voltage stress as $GX = \mathrm{Max}\{GA, GB, GC\}$, and the normalized voltage stress as $GX^* = GX/V_p$, where V_p is phase voltage amplitude of the positive-sequence triangle, like G_1A_1 in ΔA_1BC_1 in Fig. 10, namely the voltage stress under the balanced grid condition. For a given unbalance factor k, GX can also be different. Take phase A as an example, the worst case occurs when the negative-sequence vector $\mathbf{G_2A_2}$ of the phase voltage is in the same direction of the positive-sequence vector $\mathbf{G_1A_1}$ as shown in Fig. 10(b), and the phase A cluster withstands the maximum voltage stress **GA** at such given unbalance level. Since now the unbalance factor of the line voltage equals k, the voltage stress can be expressed as

$$GX = GA = G_1A_1 + G_2A_2 = V_p + V_n = (1+k)\,V_p \quad (6)$$

$$GX^* = 1 + k \quad (7)$$

Generally, equation (7) can also be applied to other clusters if the worst case happens to them. Considering that the grid current phasor and phase voltage phasor share the similar triangles, the maximum current stress occurs to the same cluster like the voltage stress does. Equation (7) can also be regarded as the expression of the current stress, where GX^* stands for the normalized current stress by the positive-sequence current component. Equation (7) shows the relationship between the normalized voltage or current stress and the unbalance factor, and it proves that the voltage and current stress of a star-connected cascade STATCOM is in linear relationship with the voltage unbalance level. For example, the device under the IPCC can withstand an additional 50% negative-sequence voltage as long as it has 0.5 times voltage stress margin.

It should be noted that this analysis focuses on the overvoltage conditions of grid voltage unbalance. In order to simplify the analysis, it is assumed that the positive-sequence voltage vectors are kept unchanged, while the unbalance condition is made by adding negative-sequence vectors. Actually, severe unbalanced conditions are mainly caused by asymmetrical short-circuit faults in which the positive-sequence voltage V_p is greatly decreased than normal, so the voltage stress is not as large as shown in equation (6). Like one line grounding (1LG) shown in Fig. 10(a), the unbalance level is less than 100%, and the phase voltage becomes even smaller than the one before fault. Hence, the voltage stress is definitely tolerable, and the STATCOM based on IPCC can function well under 1LG condition.

C. Limitation of the OZSCS Algorithm

Before analyzing the operation range and reliability of the OZSCS algorithm, the value range of the unbalance factor k should be determined first. According to the definition of k, in real power systems, the k values of almost all the conditions are not more than 100%. It can be proved mathematically that when $k = 100\%$, namely the amplitudes of positive and negative sequence are equal, three line-to-line or phase voltage phasors are collinear, and one typical case is two-line short circuit (2LS) fault which is shown in Fig. 12(b). Hence, considering k value ranges from 0 to 100%, the limitation of the OZSCS algorithm is developed as follows.

First, OZSCS is inapplicable when the unbalance factor k equals 100%. From the expression of the optimal vectors in equation (4) which is used for zero-sequence current separation, it can be found that the angle φ_x, and φ_y (or $\varphi_y + \pi$) can not be equal to (or extremely close to) each other, or the denominator of the expression is equal (or close) to zero, resulting in the consequence that the output of OZSCS will exceed the current rating or even tend to infinity. The physical implication of such constraint can be explained as follows: when the unbalance factor k equals 100%, for example, under a 2LS fault condition,

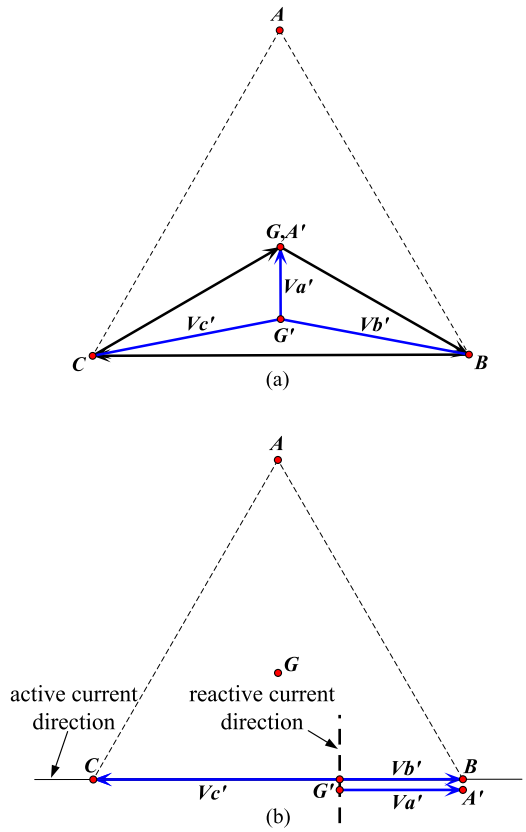

Fig. 12. Grid voltage under asymmetrical faults (G' is the new neutral point after faults). (a) 1LG (phase A is grounding). (b) 2LS (phase A and B is at short-circuit).

three line-to-line or phase voltage phasors are collinear. Three-dashed lines in Fig. 4 are also collinear and vertical with three-phase voltage phasors, and then angle φ_x and φ_y (or $\varphi_y + \pi$) in Fig. 5 are equal. The active and reactive current directions are marked in Fig. 12(b), and they are vertical to each other. It leads to the result that any changes in the reactive part of the current reference cannot counteract the zero-sequence component in the active part, and then, the sum of active and reactive current references cannot be regulated to zero. Thus, in this situation, the OZSCS algorithm outputs infinity, and the IPCC will break down.

Second, the logic of Table I in Section II-B2 is absolutely reliable when k is less than 100%. When k $<$ 100%, the amplitude of the positive-sequence voltage is larger than one of negative sequence. Hence, the phase voltage V_a always leads V_b leads V_c in sequence. Since the dashed lines aa', bb', and cc' in Fig. 4, respectively, lead their corresponding voltage V_a, V_b, and V_c by 90 degrees, line aa' leads bb' leads cc' in the same way. Thus, under this condition, the sequence of aa', bb', and cc' always agrees with the one in Fig. 4, and the logic of Table I is credible.

In conclusion, the OZSCS algorithm itself can be effective when the unbalance factor k is less than 100%. This operation range can cover most of the unbalanced conditions in real-power systems, except for the situations with $k = 100\%$ such as two-line short circuit (2LS).

TABLE II
SIMULATION PARAMETERS OF THE CASCADE STATCOM

Simulation environment	PSCAD
Rated capacity of the converter	10 Mvar
Line-to-line grid voltage (rms)	35 kV
Rated ac-output voltage of STATCOM (rms)	10 kV
Rated ac current (rms)	577 A rms
Interface Inductor L	5.2 mH
Equivalent resistance R	0.05 Ω
Number of converter cells in each cluster N	12
Rated dc voltage of each converter cell	1000 V
DC capacitance of each converter cell	7 mF
Switching frequency of each device	250 Hz
Modulation method	Phase-shifted PWM

It should be noted that with the OZSCS algorithm, some phase currents may deviate from the reference, while the tracking error of the total reactive power may not be quite large. The OZSCS algorithm is designed with the consideration that the total changes in three current references should be minimized. As illustrated in Section II-B2, the OZSCS algorithm first determines which sector the zero sequence current vector $_{-}\mathbf{I}_z{}^*$ is located in, and then utilizes the reactive segments on two edges of this sector to form $_{-}\mathbf{I}_z{}^*$. By doing so, it can be guaranteed that the total modifications of reactive current references are minimized, thus, the reactive tracking error is lowest.

IV. RESULTS

A. Simulation

A star-connected cascade STATCOM rated at ±10 Mvar/10 kV is simulated using PSCAD/EMTDC. The simulation parameters are listed in Table II.

To test the dynamic performance of the STATCOM under IPCC, the simulations are performed under this circumstance: before $t = 1.8$ s, the cascade STATCOM is providing 577-A rms reactive current to a balanced power grid; at $t = 1.8$ s, the grid voltage suddenly becomes unbalanced ($k = V_{-}/V_{+} = 38\%$); at $t = 2.2$ s, the grid voltage is back to balance. Both waveforms in Figs. 13 and 14 are obtained under IPCC, while Fig. 13 is WITH OZSCS, and Fig. 14 is WITHOUT OZSCS. Fig. 13(a) shows the waveforms of three-phase grid voltages, and the unbalance is set by an asymmetric fault. Fig. 13(b) shows the waveforms of STATCOM output currents, and the currents become distorted when the grid voltage is switching between balance and unbalance. As shown in Fig. 13(c), the total harmonic distortion (THD) of I_a increases to over 10% when the grid voltage changes, but it is back to 2% just after one-line period even when the grid voltage is still significantly unbalanced. Fig. 13(b) and (c) shows that the output current under IPCC will not be influenced by the unbalanced grid voltage. Note that the amplitude of the three-phase current becomes different under unbalanced condition, which indicates that the IPCC has the feature of NSCI. Fig. 13(d) shows the dc-side capacitor voltages of 36-H-bridge cells. Fig. 13(e) shows the equivalent dc voltage of each cluster which is the sum of 12-H-bridge cells in one cluster. When the

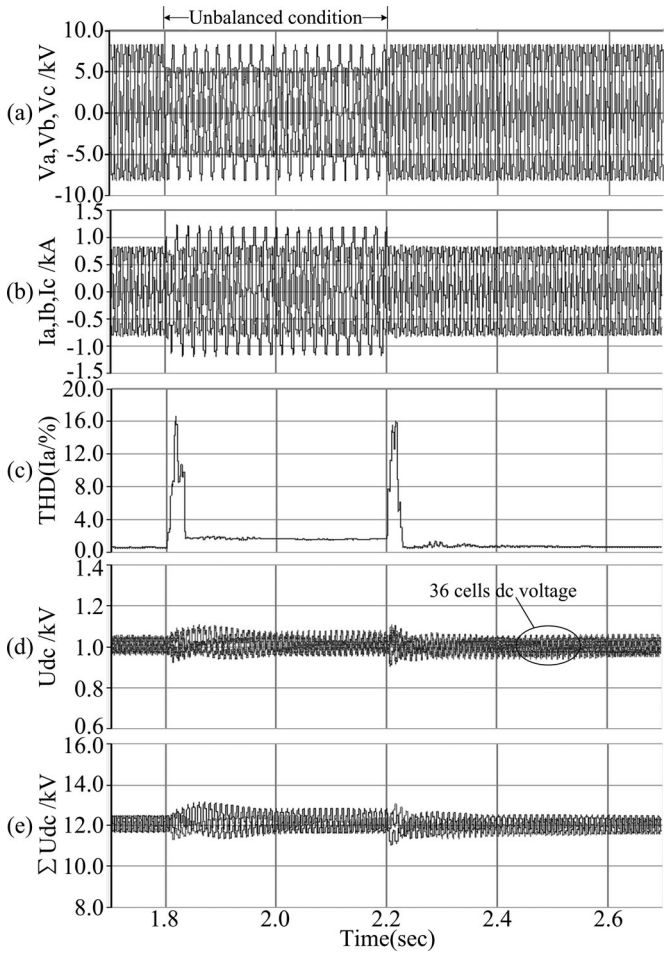

Fig. 13. Simulation waveforms of cascade STATCOM operating under unbalanced grid voltage using IPCC with OZSCS. (a) Grid voltage. (b) Output current. (c) Phase A current THD. (d) DC-side voltages of 36 H-bridge cells. (e) Summaries of dc voltages in each phase cluster.

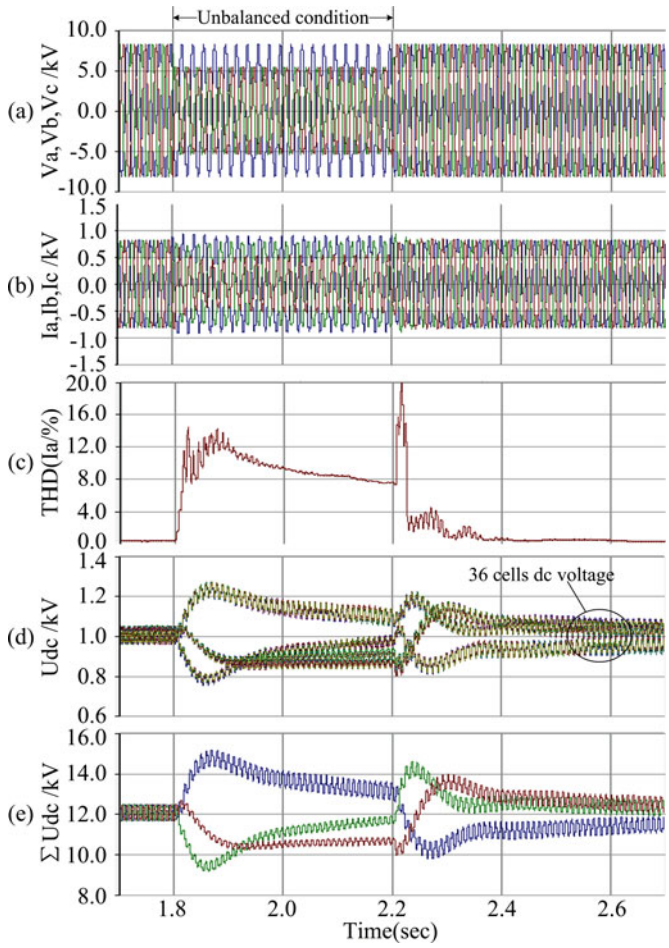

Fig. 14. Simulation waveforms of cascade STATCOM operating under unbalanced grid voltage using IPCC without OZSCS. (a) Grid voltage. (b) Output current. (c) Phase A current THD. (d) DC-side voltages of 36 H-bridge cells. (e) Summaries of dc voltages in each phase cluster.

unbalance condition occurs, the overshoots of 36-cells dc voltages are no more than 80 V, and the voltages become back to balance within 0.2 s. Fig. 13(d) (e) shows that the dc-side capacitor voltage will not be influenced by the unbalanced condition.

Zero-sequence separation is essential to IPCC. It can be demonstrated in Fig. 14 whose waveforms are got from the same simulation parameters and scenario with those in Fig. 13. Only difference is that the optimal zero-sequence current reference separation is removed. As shown in Fig. 14, the transient settling time is much longer and dc-voltage overshoots are larger than the ones in Fig. 13. Under unbalanced conditions, the output currents are greatly distorted, and the equivalent dc voltages of three clusters are quite different. However, the dc voltages in one cluster are always balanced and the STATCOM can still function. Together from Figs. 13 and 14, we can conclude

1) IPCC can make the cascade STATCOM unaffected by unbalanced conditions;
2) optimal zero-sequence current reference separation enables IPCC performed on star-connected cascade STATCOMs as well, without great current distortion.

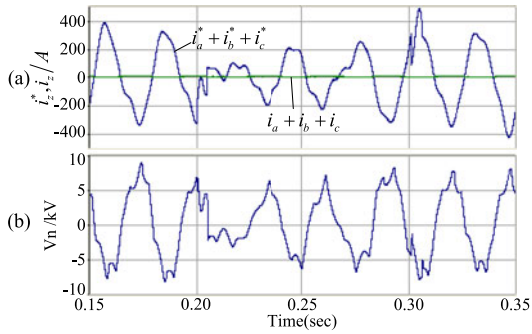

Fig. 15. Simulation waveforms of IPCC without zero-sequence current separation. (a) Sum of three-phase instantaneous currents $i_a + i_b + i_c$ and sum of three-phase current references $i_a^* + i_b^* + i_c^*$. (b) Neutral point voltage.

Waveforms in Figs. 15 and 16 provide some insight into how zero sequence separation does enable IPCC to work. Since each cluster is controlled separately, there is no mechanism to guarantee i_z^* to be zero. But in the three-wire system, i_z must always be zero. Therefore, great distortion appears in the output current, and the neutral point voltage V_N becomes greatly biased and fluctuating, causing greater disturbance to

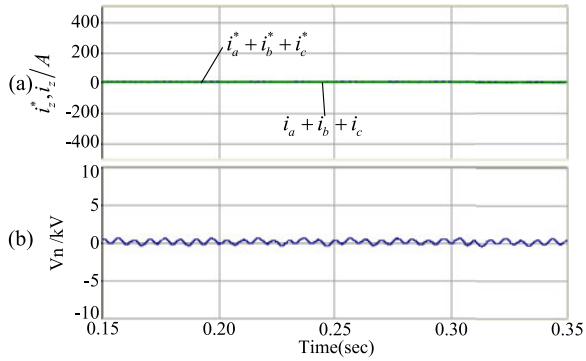

Fig. 16. Simulation waveforms of IPCC with zero-sequence current separation. (a) Sum of three-phase instantaneous currents $i_a + i_b + i_c$ and sum of three-phase current references $i_a^* + i_b^* + i_c^*$. (b) Neutral point voltage.

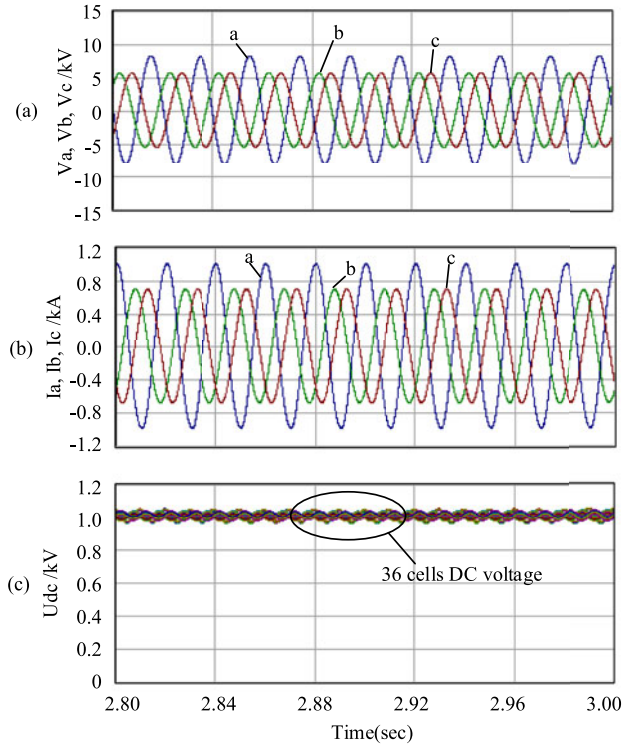

Fig. 17. Simulation waveforms of cascade STATCOM using IPCC with OZSCS when $V_-/V_+ = 30\%$. (a) Grid voltage. (b) Output current.

the current controller, as shown in Fig. 15. If the zero-sequence reference is removed before being fed into the current controller as shown in Fig. 16, then the distortion can be prevented, and the neutral voltage V_N is back to zero. It consists with the analysis in Section III that the potential of neutral is at the same point with the voltage reference O.

Waveforms in Figs. 17, 18, and 19 show the steady-state performance of IPCC based on OZSCS under different unbalance factors, namely 30%, 50%, and 90%. These simulations are performed under the same control parameters. And in order to verify the operation range analysis in Section III, largest voltage and current stress occur to phase A like the condition shown in Fig. 10(b). By measurement, the amplitude ratio of the negative- and positive-sequence components in the grid

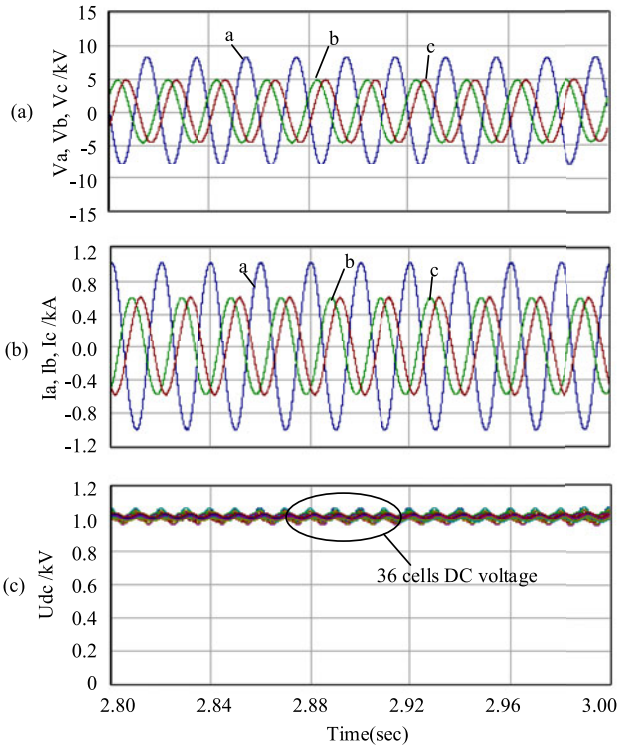

Fig. 18. Simulation waveforms of cascade STATCOM using IPCC with OZSCS when $V_-/V_+ = 50\%$. (a) Grid voltage. (b) Output current.

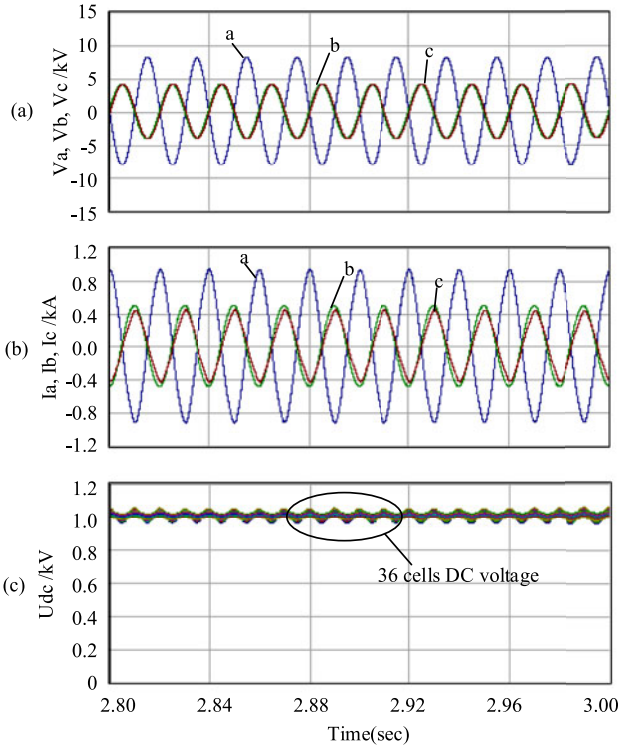

Fig. 19. Simulation waveforms of cascade STATCOM using IPCC with OZSCS when $V_-/V_+ = 90\%$. (a) Grid voltage. (b) Output current.

TABLE III
PARAMETERS OF THE CASCADE STATCOM PRODUCT

Rated capacity of the converter	10 Mvar
Line-to-line grid voltage (rms)	35 kV
Rated ac output voltage of STATCOM (rms)	10 kV
Rated ac current (rms)	577 A
Interface Inductor L:	5.2 mH
Number of converter cells in each cluster N	12
Rated dc voltage of each converter cell	1000 V
DC capacitance of each converter cell	7 mF
Switching frequency of each device	250 Hz
Switching Device	FF1000R17IE4
Modulation method	Phase-shifted PWM

Fig. 20. Cascade STATCOM used to test the proposed control.

current in three figures are respectively 0.289, 0.495, and 0.904, very close to the value of each unbalance factor k, which agrees with the theoretical analysis above. Though STATCOM under the OZSCS algorithm cannot operate under 100% unbalance, it can still function well when the unbalanced factor is close to 100% in Fig. 19. The clusters have larger current distortion under more severe unbalance, because the disturbance brought in by the floating neutral point is larger when the unbalance conditions became more serious.

B. Experiment

The proposed method is tested on a ±10-Mvar/10-kV star-connected cascade multilevel STATCOM product, which is connected to the 35-kV power line in a wind farm through a step-up transformer. The circuit configuration is shown in Fig. 1, and the parameters are listed in Table III. Fig. 20 shows a photograph of the product.

This cascade STATCOM consists of one control box and 36 full-digital-controlled H-bridge cells. Each H-bridge cell is controlled by a digital signal processor (DSP) and a complex programmable logic device. Seventy-two phase-shift carrier PWM signals are generated by field-programmable gate array of the control box and transmitted to each H-bridge cell through optical fibers. The 36 dc voltages of each cell are transmitted through a two-layer communication network to the DSPs of the control box.

The experimental results are shown in Figs. 21 and 22. The waveforms in Figs. 21(a) and 22(a) are three-phase output currents of the cascade STATCOM measured from the second side of current transformers (CTs). The turns ratio of the CTs is 120:1. Therefore, the STATCOM was working at approximately 1.7 Mvar in this experiment. The reason why not to work at full power is that the grid in this wind farm is weak, the full reactive power output can cause the ac bus overrun. Both waveforms in Figs. 21 and 22 are performed under IPCC. Fig. 21 shows the current waveform under the IPCC WITH zero-sequence separation. The current THD is 3.145%, demonstrating the effectiveness of the proposed control strategy. Fig. 22 shows the result WITHOUT OZSCS, and the current is distorted and the THD increases to 8.103%. These results together indicate that by using OZSCS, a star-connected cascade STATCOM can be controlled separately. The experiment THD values in Figs. 21 and 22 are not quite same with the simulation ones in Figs. 13 and 14 because of their different operation points. The circuit and controller parameters in the experiment and simulation are basically same, however, the STATCOM runs at 10 Mvar in simulation which is different from the experimental condition. Besides, the real-grid voltage contains much background harmonics, the voltage unbalance factor is always changing.

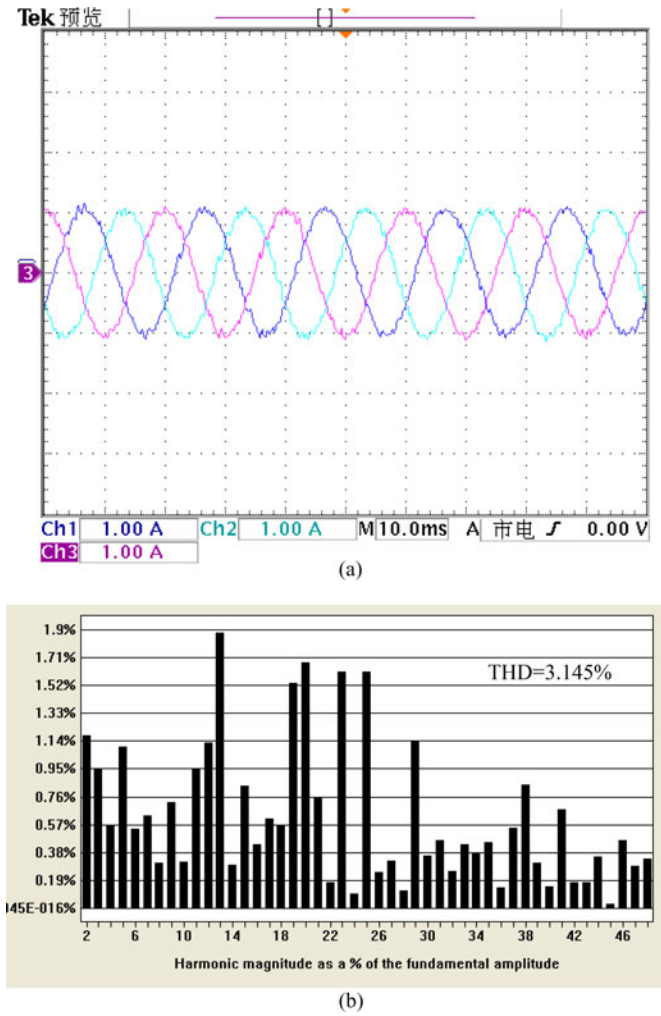

Fig. 21. Experimental waveforms of the cascade STATCOM with OZSCS. (a) Output current, ratio = 1:120. (b) Current THD.

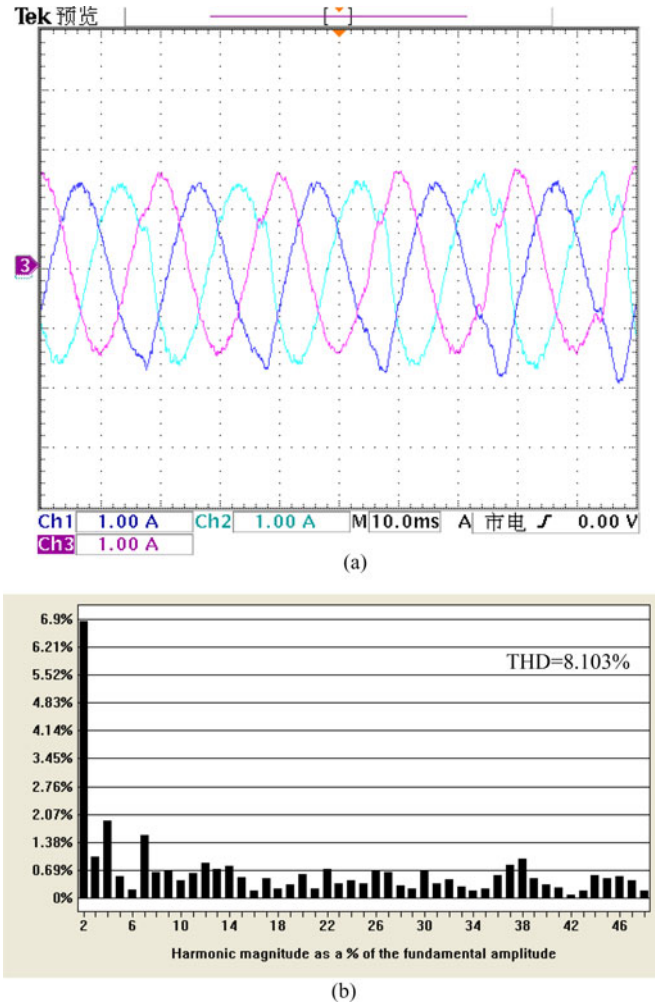

Fig. 22. Experimental waveforms of the cascade STATCOM without OZSCS. (a) Output current, ratio = 1:120. (b) Current THD.

V. Conclusion

This paper presents a new control method for star-connected cascade STATCOMs operating under unbalanced grid voltage. By applying IPCC, each cluster of the cascade STATCOM is treated as an individual converter. Namely, each cluster has its own phase current control loop and dc-voltage feedback loop. This control method generates the necessary negative-sequence current automatically to rebalance power, along with the unnecessary and harmful zero-sequence current. An OZSCS algorithm is developed to make modifications on reactive compensation component and remove the unwanted zero-sequence current reference without influencing other parts of the control; Also, an individual PLL based on virtual three-phase dq transformation is developed to obtain the instantaneous angle of each phase voltage even under unbalanced condition. The negative-sequence current proportion and voltage stress of a cascade STATCOM is in linear relationship with the grid unbalance factor. The proposed control is verified on a 25-level ± 10 Mvar/10-kV star-connected cascade STATCOM in simulation and on a real product in the wind farm. The results show that the proposed control provides the ability for cascade STATCOM operating under unbalanced grid voltage. The following key features of the proposed improved IPCC can be concluded:

1) the idea of improved IPCC is to make modifications on the reactive compensation current in order to decouple the cascade STATCOM into three individual converters;
2) it makes star-connected STATCOMs adapted to unbalanced grid automatically, without the need for identifying an unbalanced condition, switching to any special power balancing algorithm, or using positive-/negative-sequence extraction techniques.

References

[1] J. Rodríguez, J. S. Lai, and F. Z. Peng, "Multilevel inverters: A survey of topologies, controls, and applications," *IEEE Trans. Ind. Electron.*, vol. 49, no. 4, pp. 724–738, Aug. 2002.

[2] M. Malinowski, K. Gopakumar, J. Rodriguez, and M. A. Pérez, "A survey on cascaded multilevel inverters," *IEEE Trans. Ind. Electron.*, vol. 57, no. 7, pp. 2197–2206, Aug. 2009.

[3] S. Kouro, M. Malinowski, K. Gopakumar, J. Pou, L. G. Franquelo, B. Wu, J. Rodriguez, M. A. Pérez, and J. I. Leon, "Recent advances and industrial applications of multilevel converters," *IEEE Trans. Ind. Electron.*, vol. 57, no. 8, pp. 2553–2580, Jun. 2010.

[4] J. Rodríguez, S. Bernet, B. Wu, J. O. Pontt, and S. Kouro, "Multilevel voltage-source-converter topologies for industrial medium-voltage drives," *IEEE Trans. Ind. Electron.*, vol. 54, no. 6, pp. 2930–2945, Dec. 2007.

[5] T. Zhao, G. Wang, S. Bhattacharya, and A. Q. Huang, "Voltage and power balance control for a cascaded h-bridge converter-based solid-state transformer," *IEEE Trans. Power Electron.*, vol. 28, no. 4, pp. 1523–1532, Sep. 2012.

[6] D. E. Soto-Sanchez, R. Peña, R. Cárdenas, J. Clare, and P. Wheeler, "A cascade multilevel frequency changing converter for high-power applications," *IEEE Trans. Ind. Electron.*, vol. 60, no. 6, pp. 2118–2130, Apr. 2012.

[7] L. Tarisciotti, P. Zanchetta, A. Watson, S. Bifaretti, J. C. Clare, and P. W. Wheeler, "Active DC voltage balancing PWM technique for high-power cascaded multilevel converters," *IEEE Trans. Ind. Electron.*, vol. 61, no. 11, pp. 6157–6167, Feb. 2014.

[8] P. Karamanakos, K. Pavlou, and S. Manias, "An enumeration-based model predictive control strategy for the cascaded h-bridge multilevel rectifier," *IEEE Trans. Ind. Electron.*, vol. 61, no. 7, pp. 3480–3489, Aug. 2013.

[9] C. K. Lee, J. S. K. Leung, S. Y. R. Hui, and H. S. H. Chung, "Circuit-level comparison of STATCOM technologies," *IEEE Trans. Power Electron.*, vol. 18, no. 4, pp. 1084–1092, Jul. 2003.

[10] B. Gultekin, C. O. Gerçek, T. Atalik, M. Deniz, N. Biçer, M. Ermis, K. N. Kose, C. Ermis, E. Koç, I. Çadirci, A. Açik, Y. Akkaya, H. Toygar, and S. Bideci, "Design and implementation of a 154-kV $\pm$50-mvar transmission STATCOM based on 21-level cascaded multilevel converter," *IEEE Trans. Ind. Appl.*, vol. 48, no. 3, pp. 1030–1045, Mar. 2012.

[11] B. Gultekin and M. Ermis, "Cascaded multilevel converter-based transmission STATCOM: System design methodology and development of a 12 kV $\pm$12 MVAr power stage," *IEEE Trans. Power Electron.*, vol. 28, no. 11, pp. 4930–4950, Jan. 2013.

[12] F. Z. Peng, J. S. Lai, J. W. McKeever, and J. VanCoevering, "A multilevel voltage-source inverter with separate DC sources for static VAr generation," *IEEE Trans. Ind. Appl.*, vol. 32, no. 5, pp. 1130–1138, Sep.–Oct. 1996.

[13] H. Akagi, S. Inoue, and T. Yoshii, "Control and performance of a transformerless cascade PWM STATCOM with star configuration," *IEEE Trans. Ind. Appl.*, vol. 43, no. 4, pp. 1041–1049, Jul.–Aug. 2007.

[14] Q. Song, W. Liu, and Z. Yuan, "Multilevel optimal modulation and dynamic control strategies for STATCOMs using cascaded multilevel inverters," *IEEE Trans. Power Del.*, vol. 22, no. 3, pp. 1937–1946, Jul. 2007.

[15] S. Du, J. Liu, J. Lin, and Y. He, "A novel DC voltage control method for STATCOM based on hybrid multilevel h-bridge converter," *IEEE Trans. Power Electron.*, vol. 28, no. 1, pp. 101–111, May 2012.

[16] X. She, A. Q. Huang, T. Zhao, and G. Wang, "Coupling effect reduction of a voltage-balancing controller in single-phase cascaded multilevel converters," *IEEE Trans. Power Electron.*, vol. 27, no. 8, pp. 3530–3543, Feb. 2012.

[17] J. M. Guerrero, P. C. Loh, T. L. Lee, and M. Chandorkar, "Advanced control architectures for intelligent microgrids—Part II: Power quality, energy storage, and AC/DC microgrids," *IEEE Trans. Ind. Electron.*, vol. 60, no. 4, pp. 1263–1270, Apr. 2012.
[18] T. L. Lee, S. H. Hu, and Y. H. Chan, "D-STATCOM With positive-sequence admittance and negative-sequence conductance to mitigate voltage fluctuations in high-level penetration of distributed-generation systems," *IEEE Trans. Ind. Electron.*, vol. 60, no. 4, pp. 1417–1428, Aug. 2011.
[19] B. Blazic and I. Papic, "Improved D-statcom control for operation with unbalanced currents and voltages," *IEEE Trans. Power Del.*, vol. 21, no. 1, pp. 225–233, Jan. 2006.
[20] Q. Song and W. Liu, "Control of a cascade STATCOM with star configuration under unbalanced conditions," *IEEE Trans. Power Electron.*, vol. 24, no. 1, pp. 45–58, Jan. 2009.
[21] C. Han, A. Q. Huang, Y. Liu, and B. Chen, "A generalized control strategy of per-phase DC voltage balancing for cascaded multilevel converter-based STATCOM," in *Proc. IEEE Power Electron. Spec. Conf.*, 2007, pp. 1746–1752.
[22] L. Maharjan, T. Yamagishi, and H. Akagi, "Active-power control of individual converter cells for a battery energy storage system based on a multilevel cascade PWM converter," *IEEE Trans. Power Electron.*, vol. 27, no. 3, pp. 1099–1107, Jul. 2010.
[23] R. E. Betz, T. Summers, and T. Furney, "Symmetry compensation using a h-bridge multilevel STATCOM with zero sequence injection," in *Proc. IEEE Ind. Appl. Conf., 41st IAS Annu. Meeting*, 2006, pp. 1724–1731.
[24] K. Sano and M. Takasaki, "A transformerless D-STATCOM based on a multivoltage cascade converter requiring no DC sources," *IEEE Trans. Power Electron.*, vol. 27, no. 6, pp. 2783–2795, Nov. 2011.
[25] J. I. Yutaka Ota, Y. Shibano, N. Niimura, and H. Akagi, "A phase-shifted-PWM D-STATCOM using a modular multilevel cascade converter (SSBC)—Part I: Modeling, analysis, and design of current control," *IEEE Trans. Ind. Appl.*, vol. 51, no. 1, pp. 279–288, May 2014.
[26] J. I. Yutaka Ota, Y. Shibano, and H. Akagi, "A phase-shifted PWM D-STATCOM using a modular multilevel cascade converter (SSBC)—Part II: Zero-voltage-ride-through capability," *IEEE Trans. Ind. Appl.*, vol. 51, no. 1, pp. 289–296, May 2014.
[27] V. B. Bhavaraju and P. N. Enjeti, "Analysis and design of an active power filter for balancing unbalanced loads," *IEEE Trans. Power Electron.*, vol. 8, no. 4, pp. 640–647, Oct. 1993.
[28] N. Hatano and T. Ise, "A configuration and control method of cascade H-bridge STATCOM," in *Proc. IEEE Power Energy Soc. Gen. Meeting—Convers. Del. Electr. Energy 21st Century*, 2008, pp. 1–8.
[29] C. Lee, B. Wang, S. Chen, S. Chou, J. Huang, P. Cheng, H. Akagi, and P. Barbosa, "Average power balancing control of a STATCOM based on the cascaded h-bridge PWM converter with star configuration," *IEEE Trans. Ind. Appl.*, vol. 50, no. 6, pp. 3893–3901, Mar. 2014.
[30] N. Hatano and T. Ise, "Control scheme of cascaded h-bridge STATCOM using zero-sequence voltage and negative-sequence current," *IEEE Trans. Power Del.*, vol. 25, no. 2, pp. 543–550, Jan. 2010.
[31] C. Lee, H. Chen, C. Wang, P. Wu, C. Yang, and P. Cheng, "A flexible DC voltage balancing control based on the power flow management for star-connected cascaded H-bridge converter," in *Proc. IEEE Energy Convers. Congr. Expo.*, 2014, pp. 3922–3929.
[32] D. J. Hanson, "A transmission SVC for national grid company plc incorporating a ±75 MVAr STATCOM," in *Proc. IEE Colloq. Flexible AC Transmission Syst.*, 1998, pp. 5/1–5/8.
[33] C. Horwill, A. J. Totterdell, D. J. Hanson, D. R. Monkhouse, and J. J. Price, "Commissioning of a 225 Mvar SVC incorporating A ±75 Mvar STATCOM at NGC's 400 kV east claydon substation," in *Proc. 7th Int. Conf. AC-DC Power Transmission*, 2001, pp. 232–237.
[34] Y. Shi, B. Liu, and S. Duan, "Eliminating DC current injection in current-transformer-sensed STATCOMs," *IEEE Trans. Power Electron.*, vol. 28, no. 8, pp. 3760–3767, Nov. 2012.
[35] Z. Liu, Y. Shi, S. Duan, Y. Kang, and T. Chen, "The research of DC capacitance voltages balancing strategy based on cascade STATCOM using individual phase instantaneous current tracking," in *Proc. IEEE 6th Int. Power Electron. Motion Control Conf.*, 2009, pp. 1136–1140.
[36] S. Wang, Y. Li, P. Wang, P. Song, L. Tan, H. Ren, and J. Liu, "Hierarchical design and control of 10kV/1Mvar cascade STATCOM," in *Proc. IEEE 9th Conf. Ind. Electron. Appl.*, 2014, pp. 1319–1323.
[37] J. Wu, Q. Chen, M. Du, and S. Yu, "Sliding-mode variable structure controller for cascade STATic var COMpensator," *IET Power Electron.*, vol. 6, no. 2, pp. 343–352, 2013.
[38] Z. Liu, B. Liu, S. Duan, and Y. Kang, "A novel DC capacitor voltage balance control method for cascade multilevel STATCOM," *IEEE Trans. Power Electron.*, vol. 27, no. 1, pp. 14–27, May 2010.
[39] *Testing and Measurement Techniques-Section 30: Power Quality Measurement Methods*, IEC Standard 61000-4-30, 2003.

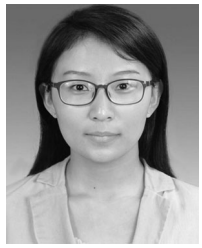

Youjie Shi received the B.S. degree in electrical engineering and automation from the Huazhong University of Science and Technology, Wuhan, China, in 2012, where she is currently working toward the Ph.D. degree in the School of Electrical and Electronics Engineering.

Her research interests include renewable energy applications and large-capacity inverters.

Bangyin Liu (M'10) received the B.S., M.S., and Ph.D. degrees in electrical engineering from the Huazhong University of Science and Technology (HUST), Wuhan, China, in 2001, 2004, and 2008, respectively.

He was a Postdoctoral Research Fellow with the Department of Control Science and Engineering, HUST, from 2008 to 2010. He is currently an Associate Professor with the School of Electrical and Electronics Engineering, HUST. His current research interests include renewable energy applications, power quality, and power electronics applied to the power system.

Yanjun Shi (S'10–M'12) received the B.S. and Ph.D. degrees in electrical engineering from the Huazhong University of Science and Technology, Wuhan, China, in 2007 and 2012, respectively.

He is currently working as a Postdoctoral Researcher in the Center for Advanced Power System, Florida State University, Tallahassee, FL, USA. His current research interests include grid-connected PV system, high-power density PV inverter, high-PV penetration integration issues, widebandgap device application, and modeling and control of modular multilevel converter.

Shanxu Duan received the B.Eng., M. Eng., and Ph.D. degrees in electrical engineering from the Huazhong University of Science and Technology, Wuhan, China, in 1991, 1994, and 1999, respectively.

Since 1991, he has been a Faculty Member in the College of Electrical and Electronics Engineering, Huazhong University of Science and Technology, where he is currently a Professor. His research interests include stabilization, nonlinear control with application to power electronic circuits and systems, fully digitalized control techniques for power electronics apparatus and systems, and optimal control theory and corresponding application techniques for high-frequency pulsewidth-modulation power converters.

Dr. Duan is a senior member of the Chinese Society of Electrical Engineering and a Council Member of the Chinese Power Electronics Society. He was selected as one of the New Century Excellent Talents by the Ministry of Education of China in 2007. He received the honor of "Delta Scholar" in 2009.